Dust grain charging and levitation in a weakly collisional sheath

S. Robertson[a)]
Department of Physics, University of Colorado, Boulder, Colorado 80309-0390
and Laboratory for Atmospheric and Space Physics, University of Colorado, Boulder, Colorado 80309-0392

A. A. S. Gulbis and J. Colwell
Laboratory for Atmospheric and Space Physics, University of Colorado, Boulder, Colorado 80309-0392

M. Horányi
Department of Physics, University of Colorado, Boulder, Colorado 80309-0390
and Laboratory for Atmospheric and Space Physics, University of Colorado, Boulder, Colorado 80309-0392

(Received 11 February 2003; accepted 28 July 2003)

An experiment is described in which monodisperse dust grains are levitated within a dc sheath above a conducting plate in argon plasma. For plate bias voltages that are not too negative ($\geqslant -10$ electron temperatures), the observed dust levitation heights are near to values calculated from a model combining equations for the sheath with those for grain charging. When the plate is more negatively biased, the theoretical levitation heights are higher than the observed heights as a consequence of the measured sheath thickness being smaller than values obtained from the models.
 [DOI: 10.1063/1.1612941]

I. INTRODUCTION

Dust in plasma[1] is most easily observed within a sheath because the balancing of the electric and gravitational forces often results in stationary particles. The grains charge to a negative potential at which the incident currents of electrons and ions are equal and opposite. Near the lower boundary of the discharge, there is usually a downward pointing sheath electric field that increases as the boundary is approached. The electric force, however, may increase, decrease, or reverse in sign depending upon the grain charge. If the dust particles are not too massive, the upward electric force may cancel the gravitational force and the dust particles may be levitated. In this work, an experiment is described in which monodisperse grains are levitated in a dc discharge in argon. Levitation heights and sheath potential profiles are measured. These are compared with calculated values from a model that combines equations for the sheath potential profile with the grain charging equations. There is considerable experimental literature on the levitation of dust in RF discharges where strong coupling of the levitated dust particles results in a variety of interesting crystalline[2–5] and wave phenomena.[6,7]

There are numerous theoretical[8–14] and computational models[15,16] of the dc sheath with varying degrees of complexity. While there are a number of collisional sheath models,[17–19] we use the collisional sheath of Riemann[12] because the mean free path in the experiment is too long for a fully collisional model. The Riemann model replaces the freely accelerating ions in the Bohm collisionless model[8] with an equation of motion for the ions that includes charge-exchange collisions. In Secs. II A and II B below we combine the collisionless and collisional sheath models with the sheath charging equations. In Sec. II C these equations in dimensionless form are solved numerically for the grain charge and electric force as a function of distance from the boundary. Two equilibria are found for boundaries that are sufficiently negative, one of which is stable. An expression is derived for the largest grain that will levitate. In Sec. III, an experiment is described in which the sheath potential profile is measured and monodisperse plastic spheres 10 μm in diameter are levitated in a dc discharge above a plate that is electrically biased. The levitation heights are measured as a function of the plate bias potential. We find that the data agree with the model at the least negative bias voltages and overestimate the levitation height at large negative voltages. A summary and conclusion are presented in Sec. IV.

II. SHEATH MODELS

A. Models for the sheath

In the Bohm sheath model, there is a sheath–plasma interface at z_o and the ion velocity at the sheath–plasma interface is equal to the ion sound speed $c_s=(T_e/m_i)^{1/2}$ where T_e is the electron temperature in energy units and m_i is the ion mass. The ion temperature is assumed negligible in comparison with T_e and conservation of energy for ions requires that the potential at z_o be $\Phi(z_o)=\Phi_p-T_e/2e=\Phi_o$ where e is the elementary charge and the plasma potential is Φ_p. The ion velocity at other locations is also given by energy conservation

$$u_i(z)^2=c_s^2+\frac{2e}{m_i}[\Phi_o-\Phi(z)]=\frac{2e}{m_i}[\Phi_p-\Phi(z)]. \qquad (1)$$

The electron density is assumed to be determined by the Boltzmann relation

$$n_e(z)=n_o e\,\exp\left\{\frac{e}{T_e}[\Phi(z)-\Phi_p]\right\}, \qquad (2)$$

[a)]Electronic mail: robertso@stripe.colorado.edu

where n_o is the plasma density. The electron and ion density at z_o is reduced to $n_o \exp(-0.5) \cong 0.6\, n_o$. The ion saturation current density directed toward the boundary is then $J_{\text{sat}} = 0.6 n_o e c_s$ and the continuity equation then requires that

$$n_i(z) = \frac{J_{\text{sat}}}{e u_i(z)} = \frac{0.6 n_o c_s}{\left[\frac{2e}{m_i}[\Phi_p - \Phi(z)]\right]^{1/2}}, \quad \Phi(z) < \Phi_o . \tag{3}$$

The potential variation in the sheath is found by solving Poisson's equation

$$\epsilon_o \frac{d^2\Phi(z)}{dz^2} = -\frac{J_{\text{sat}}}{u_i(z)} + n_o e \exp\left\{\frac{e}{T_e}[\Phi(z) - \Phi_p]\right\}, \tag{4}$$

with the boundary conditions $\Phi(z_o) = \Phi_o$ and $E(z_o) = 0$, where $E(z_o)$ is the electric field at the sheath–plasma interface.

In weakly ionized plasmas, the shortest collisional distance scale is usually the ion charge-exchange mean free path. These collisions can be modeled as the loss of momentum at the rate $-\nu_c m_i u_i(z)$, where ν_c is the charge-exchange collision frequency. The ion equation of motion in the fluid approximation is then[12]

$$m_i u_i(z) \frac{du_i(z)}{dz} = -e \frac{d\Phi(z)}{dz} - \nu_c m_i u_i(z). \tag{5}$$

The potential variation in the sheath can be found numerically by integration of Eqs. (4) and (5).

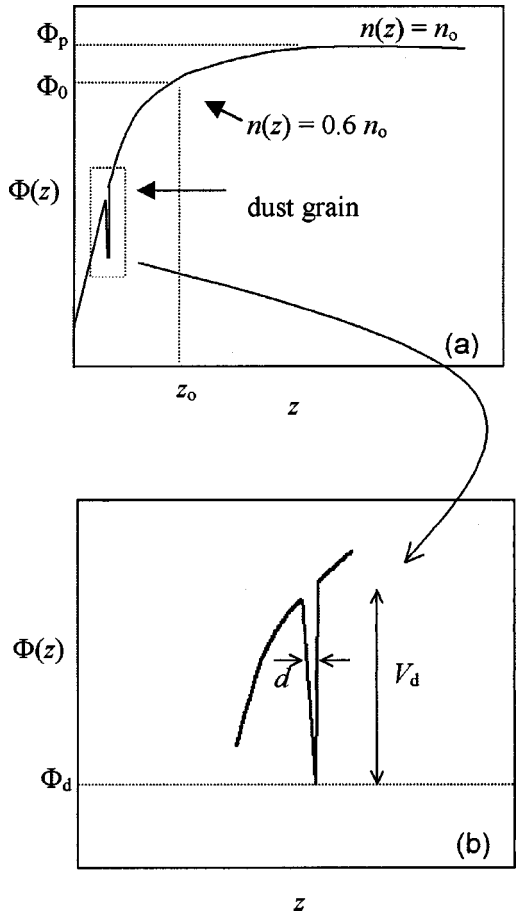

FIG. 1. (a) Diagram of the sheath model. (b) Detail of the potential perturbation in the sheath caused by a grain.

B. Grain charging

The perturbation made to the sheath potential by the charged grain is assumed to have a spatial extent d that is much greater than the grain radius and much less than the sheath width as shown in Fig. 1. The potential at the surface of the grain Φ_d falls in the distance d to the potential in the nearby sheath. The relation between the grain charge $Q(z)$, the grain potential and the potential in the nearby sheath is obtained from integration of Gauss's law:

$$\begin{aligned} Q(z) &= 4\pi\epsilon_o a[1 - a/d][\Phi_d(z) - \Phi(z)] \\ &\cong 4\pi\epsilon_o a[\Phi_d(z) - \Phi(z)], \end{aligned} \tag{6}$$

where a is the radius of the grain. This may also be written as $Q(z) = C\, V_d(z)$ where $C \cong 4\pi\epsilon_o a$ is the gain capacitance and $V_d(z) = \Phi_d(z) - \Phi(z)$ is the potential of the grain relative to the surrounding sheath plasma.

A grain at a more negative potential than $\Phi(z)$ repels electrons and the incident electron current is

$$I_e(z) = -\frac{1}{4} n_o e A u_e \exp\left\{\frac{e}{T_e}[\Phi(z) - \Phi_p]\right\}, \tag{7}$$

where $u_e = (8\, T_e/\pi m_e)^{1/2}$, m_e is the electron mass and $A = 4\pi a^2$ is the grain surface area.

For the collisionless sheath, the ion current density $J_{\text{grain}}(z)$ is found from orbit-motion-limited theory of probes[20,21]

$$J_{\text{grain}}(z) = J_{\text{sat}}\left[1 + \frac{e[\Phi(z) - \Phi_d(z)]}{K}\right], \tag{8}$$

where the bracketed term is the focusing factor and $K = \frac{1}{2} m_i u_i^2(z) = e[\Phi_p - \Phi(z)]$ is the kinetic energy of the ions in the sheath before encountering the grain potential. The equilibrium charge is reached at the grain potential for which $I_e(z) + I_i(z) = 0$, or

$$-\left[\frac{8 m_i}{\pi m_e}\right]^{1/2} \exp\left[\frac{e(\Phi_d(z) - \Phi_p)}{T_e}\right] + 0.6\left[1 + \frac{[\Phi(z) - \Phi_d(z)]}{[\Phi_p - \Phi(z)]}\right] = 0. \tag{9}$$

This expression allows the grain potential to be found as a function of the local potential $\Phi(z)$ and the potentials Φ_o and Φ_p. In the sheath literature, Φ_o is often set to zero and in the dusty plasma literature Φ_p is often set to zero. The equations here are in the most general form to avoid ambiguity.

The model for the collisional sheath is a fluid model in which u_i is the fluid velocity of the ions. In order to find the ion current in the collisional case, we calculate the ion kinetic energy from the fluid velocity and obtain from Eq. (8)

$$I_i(z) \cong \frac{A}{4} J_{\text{sat}}\left[1 + \frac{2e[\Phi(z) - \Phi_d(z)]}{m_i u_i(z)^2}\right]. \tag{10}$$

The grain charging equation for the collisional sheath is then

$$-\left[\frac{8m_i}{\pi m_e}\right]^{1/2}\exp\left[\frac{e(\Phi_d(z)-\Phi_p)}{T_e}\right] + \frac{J_{\rm sat}}{n_o e c_s}\left[1+\frac{2e[\Phi(z)-\Phi_d(z)]}{m_i u_i(z)^2}\right]=0. \quad (11)$$

For numerical solutions it is convenient to cast the collisional sheath equations into dimensionless form

$$\frac{d^2\tilde{\Phi}(\tilde{z})}{d\tilde{z}^2} = -\frac{\tilde{J}_{\rm sat}}{\tilde{u}_i(\tilde{z})} + \exp[\tilde{\Phi}(\tilde{z})], \quad (12)$$

$$\tilde{u}_i(\tilde{z})\frac{d\tilde{u}_i(\tilde{z})}{d\tilde{z}} = -\frac{d\tilde{\Phi}(\tilde{z})}{d\tilde{z}} - \eta\tilde{u}_i(\tilde{z})^2, \quad (13)$$

where the new variables are $\tilde{\Phi}(z)=e[\Phi(z)-\Phi_p]/T_e$, $\tilde{J}_{\rm sat}=J_{\rm sat}/n_o e c_s=0.6$, $\tilde{u}_i(z)=u_i(z)/c_s$, $\tilde{z}=z/\lambda_D$ and $\lambda_D=[\epsilon_o T_e/n_o e^2]^{1/2}$. The collisionality is expressed by the parameter $\eta=\lambda_D/\lambda_i$ where $\lambda_i=c_s/\nu_c$ is the charge exchange mean free path. This differs from Riemann's[12] dimensionless form because the usual Debye length has been used rather than the Debye length calculated at the sheath interface where $n_e=0.6n_o$. The boundary conditions for integration are $\tilde{\Phi}(z_o)=-0.5$, $\tilde{u}_i(z_o)=1$, and $\tilde{E}(z_o)=\eta$. The last condition is the electric field necessary to balance the collisional drag force.

The grain charging equation in dimensionless form becomes

$$-\tilde{J}_e\exp[\tilde{\Phi}_d(\tilde{z})]+\tilde{J}_{\rm sat}\left\{1+\frac{2[\tilde{\Phi}(\tilde{z})-\tilde{\Phi}_d(\tilde{z})]}{\tilde{u}_i(\tilde{z})^2}\right\}=0, \quad (14)$$

where $\tilde{J}_e=(8m_i/\pi m_e)^{1/2}$. In the collisionless case, the ion velocity is from energy conservation and in the collisional case it is from integration of Eq. (13).

C. Numerical solutions

The numerical solutions to the sheath models are shown in Fig. 2(a). For the collisional model, $\eta=0.1$ and $\eta=0.01$ are assumed. Integration is begun at $\tilde{\Phi}(z_o)=-0.5$ with $\tilde{E}(z_o)=\eta$ and continued until $\tilde{\Phi}(z)=-10$. The solutions are shifted in z so that the boundary is at zero and the position of the sheath–plasma interface is then determined by the sheath thickness. The sheath thickness is 10.3 for the collisional sheath with $\eta=0.1$ and is 16.0 for the collisional sheath with $\eta=0.01$, measured from $\tilde{\Phi}(z)=-10$ to -0.5. The collisionless sheath approaches $\tilde{\Phi}(z)=-0.5$ asymptotically and the presheath is infinitely distant. In the collisional models, the ion velocity [Fig. 2(b)] is significantly reduced with the final ion kinetic energy for $\eta=0.1$ being about a third of that given by energy conservation. The collisionality parameter alone is misleading about the effect of collisions. The probability of a charge-exchange collision in the sheath is near unity with $\eta=0.1$ because the sheath thickness is nearly ten Debye lengths.

Figure 3(a) shows the dust potential $\tilde{\Phi}_d(z)$, the sheath potential $\tilde{\Phi}(z)$ and the grain charging potential $\tilde{V}_d(z)$ for the collisional sheath with $\eta=0.1$ and Fig. 3(b) shows the corresponding electron and ion densities. The grain becomes more negative as the boundary is approached. However, the sheath potential becomes more negative than the grain potential and the charge on the grain becomes positive. Figure 4(a) shows

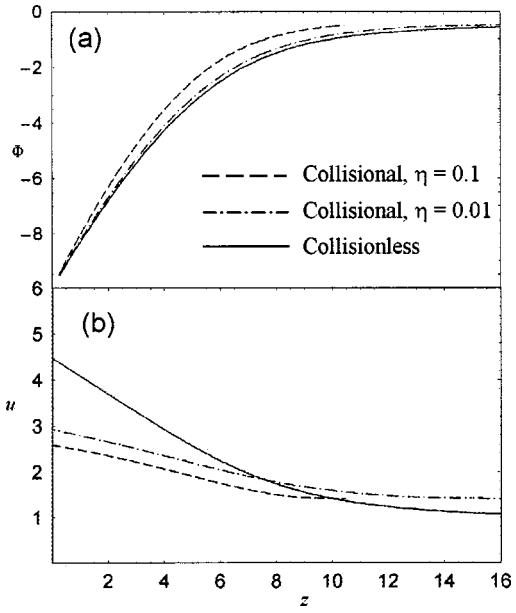

FIG. 2. (a) The potential as a function of distance from the boundary for the collisional ($\eta=0.1$ and $\eta=0.01$) and collisionless sheath models. (b) The ion velocity as a function of distance from the boundary for the three sheath models. The units for both graphs are dimensionless.

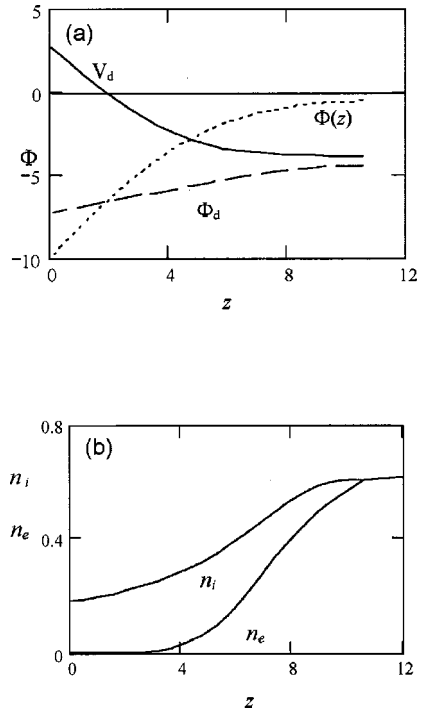

FIG. 3. (a) The sheath potential $\Phi(z)$, the dust potential Φ_d, and the grain charging potential relative to the sheath, V_d, as a function of distance from the boundary. (b) The electron and ion densities as a function of distance from the boundary. Their values are 0.6 at the sheath–plasma interface. Both graphs are for the collisional model with $\eta=0.1$, and the units are dimensionless.

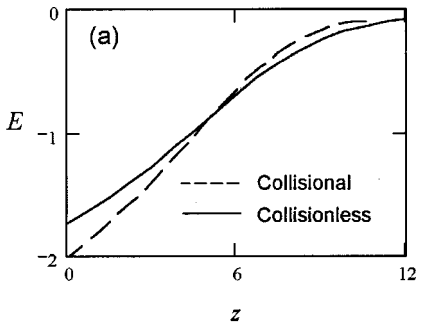

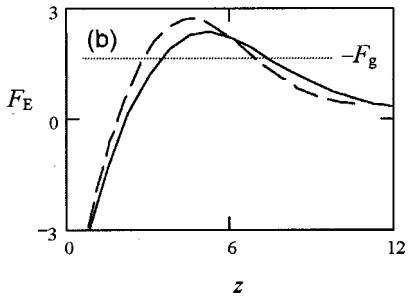

FIG. 4. (a) The sheath electric field as a function of distance for the collisional and collisionless models. (b) The electric force on the grain as a function of distance from the boundary. The units are dimensionless except for the electric force, which is in arbitrary units. The horizontal dotted line is a representative magnitude of the gravitation force.

that the sheath electric field in the collisional model is greater near the boundary than in the collisionless model and is smaller near the sheath–plasma interface. The electric force obtained from the product of the grain charge and the electric field is shown in Fig. 4(b). A representative value for the magnitude of the gravitational force F_g is shown as a dotted line. There are two possible levitation points where the electric force is equal to the magnitude of the gravitational force. The point further from the boundary is stable because the net force is toward this point if the particle is slightly displaced in either direction. The other equilibrium point is unstable. The only stable equilibria are at points where $\Phi(z)$ is less negative than about $-3\,T_e/e$. If the particle is too massive, there are no equilibria because the electric force is everywhere smaller than the gravitational force. Similar results for both collisional and collisionless sheath models have also been obtained by Nitter.[22]

For the low collisionality of our experiment, $\eta \cong 0.01$, the collisional and collisionless models do not differ significantly [Fig. 2(a)]. For this case there is a peak in the force on the grain at a distance of $5.3\,\lambda_D$ from the boundary when the potential there is $-10\,T_e/e$. At the point where the force is a maximum, the sheath potential is $-3.1\,T_e/e$, the dust potential relative to the surrounding sheath is $-2.8\,T_e/e$ and the sheath electric field is $-0.83\,T_e/e\lambda_D$. If the boundary is made less negative, then the spatial profile of the force moves toward the boundary and is otherwise unaltered. If the boundary is made more negative, the profile moves away. The peak force is unchanged by altering the boundary potential, thus the size of the particles that can be levitated is not

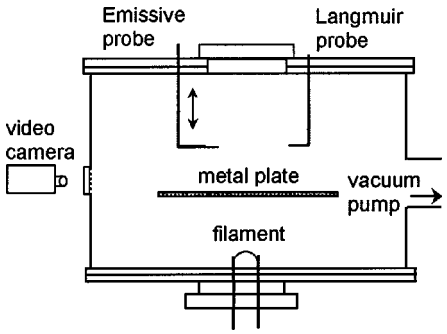

FIG. 5. Schematic drawing of the apparatus. Plasma is created in argon gas by primary electrons from the filament at the bottom of the apparatus. The dust levitates in the sheath above a metal plate that may be electrically biased. A vertical sheet of laser light transverse to the plane of the drawing illuminates the dust.

increased by making the boundary more negative. The maximum size of grain that will be levitated can be found by equating the gravitational force

$$F_g = \tfrac{4}{3}\pi\rho g a^3, \tag{15}$$

with the electric force evaluated at its maximum

$$F_E = [QE]_{\max} \cong 4\pi\epsilon_o a[2.8\,T_e/e][0.83\,T_e/(e\lambda_D)]$$

$$\cong \frac{29 a \epsilon_o T_e^2}{e^2 \lambda_D}, \tag{16}$$

where ρ is the density of the grain material and g is the acceleration of gravity. The maximum radius that can be levitated is

$$a_{\max} \cong \left(\frac{6.9\epsilon_o}{\lambda_D \rho g}\right)^{1/2} \frac{T_e}{e}. \tag{17}$$

III. EXPERIMENTS

A. Apparatus

The experiments are performed in a stainless steel vacuum chamber 51 cm in diameter and 28 cm in height (Fig. 5). The chamber is evacuated to a base pressure 3×10^{-7} Torr by a turbomolecular pump and the working pressure is 1.5×10^{-4} Torr of argon. The charge exchange cross section[23] at low energies ($\sim$0.1 eV) is $7.2 \times 10^{-15}\,\mathrm{cm}^2$ and thus the charge exchange mean free path is 26 cm. The plasma is generated by primary electrons from a filament emitting 350 mA and biased to -40 V. A few cubic millimeters of dust is placed upon a stainless steel plate 20 cm in diameter positioned approximately in the center of the vacuum chamber. This plate is electrically isolated and may float or be biased. There is a raised lip ($\sim$6 mm height) at the circumference of the plate to keep the dust from moving past the edge.

The filament is located below the plate and the collection of primaries by the plate results in a more negative floating potential for the plate than for dust particles. There is no surface magnetic containment of the primary electrons thus they follow nearly linear trajectories from the filament to the walls or the lower side of the plate. The primary electrons

thus are not present in the volume immediately above the plate and do not directly affect the grain charging, the sheath potential profile, or the probe diagnostics. The experiment is otherwise similar to that of Arnas *et al.*[24,25] in which both the plate and the grains are charged by primaries as well as plasma electrons.

Basic plasma parameters are determined by a circular, planar probe located 8 cm above the plate. The space potential $\Phi(z)$ is determined by an emissive probe nearly identical to that described by Diebold *et al.*[26] The filament heating is adjusted such that the probe emits $\sim 50\ \mu$A when several volts more negative than the local potential. A control circuit adjusts the bias voltage to the point where the emission current just exceeds a threshold ($-1\ \mu$A) and this bias voltage is recorded as $\Phi(z)$. The filament heating current is half-wave rectified AC and the data are recorded at the end of the heating pulse in order to minimize the effect of the filament voltage drop. The emissive probe may also be scanned in the same way as the Langmuir probe. The translation stage that moves the probe creates a train of electrical pulses that triggers the data taking at 0.5 mm intervals. There is an uncertainty in the probe position of ± 2 mm due to flexure of the supports. This technique has previously been used for experimental studies of the potential profiles in sheaths[27,28] and presheaths.[29–31]

Dust grains levitated in the plasma sheath are monodisperse polystyrene divinylbenzene beads $10.0 \pm 0.5\ \mu$m in diameter, a density of $1.05 \times 10^3\ \mathrm{kg/m^3}$, and a mass of 5.5×10^{-13} kg, which gives a gravitational force of $F_g = 5.6 \times 10^{-12}$ N. These grains are sufficiently large to be easily seen in the video images. Grains can be raised into the sheath by striking the plate using an insulated hammer on a vacuum feedthrough but this is not necessary at plate biases more negative than approximately -27 V. An argon laser illuminates the grains and a charge-coupled device (CCD) camera viewing through a laser line filter (488 ± 2 nm) records positions. A cylindrical lens is used to create a vertical sheet of laser light that illuminates grains at a fixed distance from the camera. A movable scale within the vacuum chamber is used to calibrate the scale of the video images and to determine the levitation heights.

Equation (17) for the conditions of the experiments gives a maximum dust levitation radius of 6.1 μm, which is consistent with the observation that 5.0 μm radius polystyrene grains are levitated. Equation (17) is also consistent with the results of experiments using monodisperse polystyrene divinylbenzene beads $7.45 \pm 0.3\ \mu$m in radius ($14.9 \pm 0.6\ \mu$m diameter), in which no particles are seen levitating. Larger hollow glass microballoons are easily levitated, however, these have a large uncertainty in mass due to variation in the wall thickness.

B. Data

For standard operating conditions, the Langmuir probe indicates an electron temperature of 3.6 (± 0.2) eV, a plasma potential of ~ 1.7 eV, a density of $2\,(\pm 1) \times 10^7\ \mathrm{cm^{-3}}$, and an average Debye length of 3.15 mm (± 1 mm). The ratio of the Debye length to the charge exchange mean free path is $\eta = 0.012$.

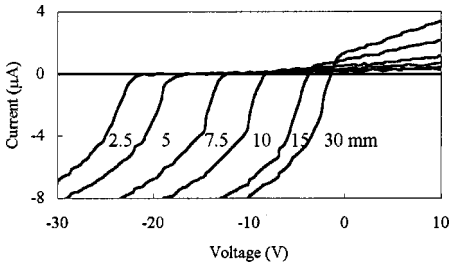

FIG. 6. Data from sweeping the emissive probe voltage and measuring the current at six distances from the plate.

Scanning the emissive probe over voltage and measuring the current at different locations, shown in Fig. 6, illustrates the use of the current bias method to measure space potential. At positive voltages the probe collects plasma electrons and at sufficiently negative voltages it emits electrons. The space potential is often interpreted as the voltage for which the curve has the greatest slope (the inflection point method).[32] An alternate technique is to use the point at which the emission crosses a threshold ($-1\ \mu$A) small in comparison with the thermionic emission limit. Comparison of these techniques for our experiment shows that the floating potentials they give differ by less than 0.2 V within the sheath. Potentials measured using the current bias method may be offset from the true potentials as a consequence of contact potentials. However, the mathematical expressions in Sec. II are written in terms of potential differences so that a constant offset in measured potentials does not affect the results of the calculations.

There was initial concern that dust particles would move away from the center of the surface as a consequence of the sheath tending to become hemispherical at large bias voltages. Figure 7 shows radial scans of the floating potential 1.5 cm above the plate at three bias voltages, which indicates that the potential contours are nearly planar. This is consistent with the observation that the dust floats stably above the central region of the plate.

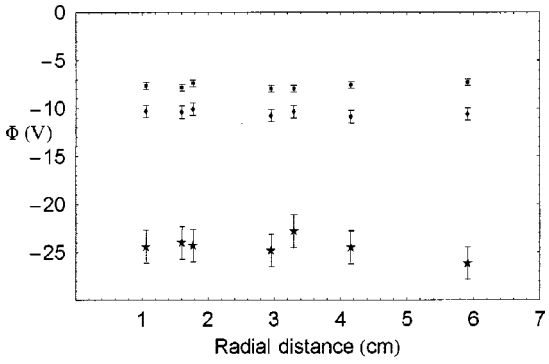

FIG. 7. Measured potential, $\Phi(z)$, at approximately 1.5 cm above the plate as a function of radial distance from the plate center. Data for three different plate biases are shown: $V_b = -30$ V (boxes), $V_b = -40$ V (diamonds), and $V_b = -80$ V (stars).

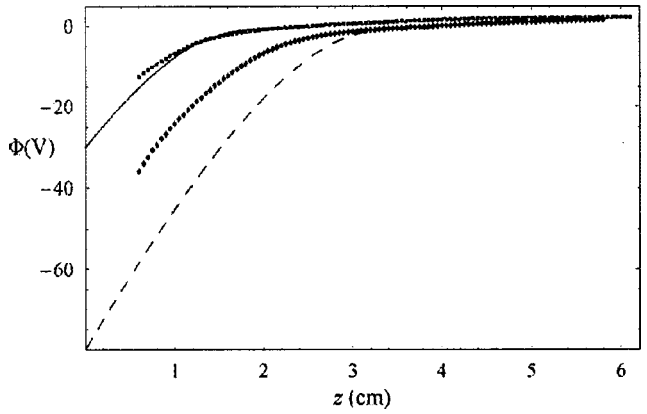

FIG. 8. Measured potential as a function of distance from the plate, $\Phi(z)$, (data points) and the potential calculated from the Riemann collisional theory with $\eta=0.012$ (lines) for two different plate biases. The square points and solid line correspond to a plate bias of -30 V, while the diamond points and the dashed line correspond to a plate bias of -80 V. The difference between the data and the theoretical curves increases as the plate bias is decreased.

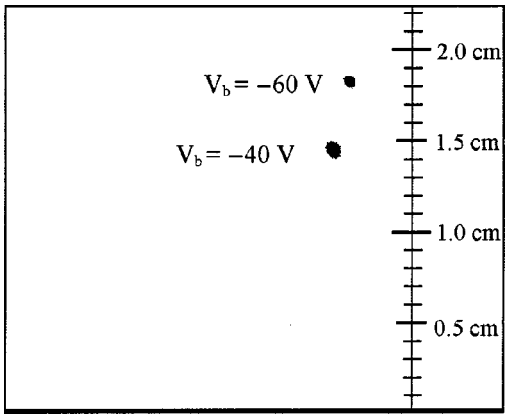

FIG. 9. Negative of two superimposed digital photographs showing a stable, levitated polystyrene grain (10.0 μm in diameter) above a plate biased to -40 and -60 V. The scale gives the distance above the plate. As expected, levitation height increases as the plate potential decreases.

The sheath potential profile above the plate measured with the emissive probe using the current bias method is shown in Fig. 8, along with the calculated sheath potential profile from the collisional model with $\eta=0.012$. The data are for the plate bias, V_b, adjusted to -30 V, which is slightly more negative than the floating potential, and to -80 V, the most negative plate bias used in the experiments. The dimensionless potential is scaled using the measured electron temperature and the plasma potential. The data and the theory for -30 V overlap visually if the measured profile is shifted toward the plate by 1 mm, which is within the uncertainty in the probe distance scale. The collisional model thus provides a good description of the measured sheath potential profile at a bias of -30 V. For bias voltages $\leqslant -30$ V, the model is found to overestimate the sheath thickness as demonstrated by the discrepancy between the data and the theoretical curve at $V_b=-80\,\mathrm{V}$ (Fig. 8). Plate bias voltages $\geqslant -30$ V were not investigated because it was difficult to obtain levitation of the 10 μm diameter particles.

An image of stably levitated dust grains is shown in Fig. 9. When measuring levitation height, the number of grains was limited so that the sheath conditions would not be altered by the presence of the grains. Two images of a single, 10.0 μm diameter, polystyrene grain are combined in Fig. 9 to show the levitation heights at plate biases of -40 and -60 V. Measured levitation heights as a function of plate biases voltages from -30 to -80 V are plotted in Fig. 10 along with levitation heights calculated in two ways: From the measured potential profile[33] and from the profile calculated using the collisional theory with $\eta=0.012$. In the first case, the measured potential profile is differentiated to find the electric field profile. The charge is calculated from Eq. (14) using the measured plasma parameters and the height is then found for which the forces cancel. The levitation heights calculated using this method are consistent with the measured levitation heights, and the exponential term in Eq. (14) results in the grain charge being relatively insensitive to errors in measurement of plasma parameters. In the second case, the measured density and temperature from the Langmuir probe are used with the Riemann collisional sheath theory to calculate a sheath potential profile. This method results in a dust levitation height which agrees with the measured height at $V_b=-30\,\mathrm{V}$, but provides a poor prediction of the dust levitation heights at the most negative bias voltages because the predicted potential profiles do not agree with the measured profiles (Fig. 8).

The discrepancy between the measured and calculated sheath profiles at increasingly negative plate biases could be a consequence of the ion density in the sheath being higher than predicted, thus giving a smaller characteristic length scale. This possibility was investigated by measuring the current density to the plate. For this measurement, a blocking surface was placed under the plate to prevent collection of plasma electrons and primary electrons by the lower side of the plate. In this situation, the current collected by the plate, Fig. 11, was found to increase with bias voltage. The ion current density J_{sat} used in the sheath theories does not vary with plate bias potential. For the least negative bias voltages, the saturation current is nearest to the measured current and the sheath profile is near to that calculated from the theory. For the most negative bias voltages, the measured current

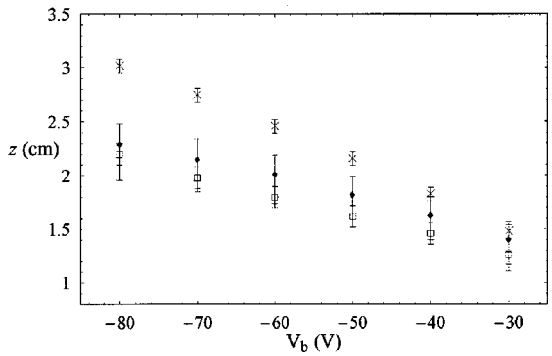

FIG. 10. Levitation height of a single 10 μm diameter polystyrene dust particle as a function of plate bias, V_b. The hollow boxes represent heights measured in the experiment, the diamonds are calculated using an exponential fit to the sheath data, and the $\times$ marks are calculated using the Riemann collisional theory for the sheath.

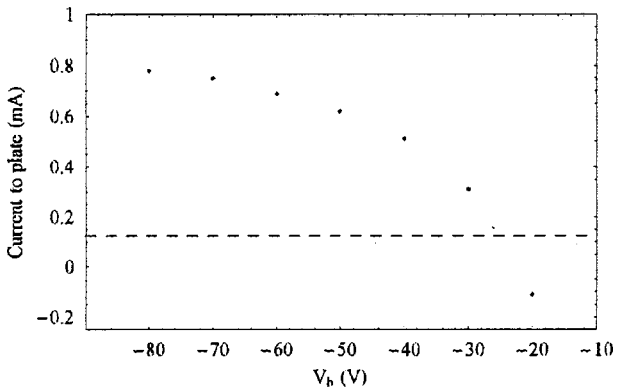

FIG. 11. The measured current to the plate as a function of the bias potential. The saturation current is represented by the dotted line.

density is significantly larger than in the model, thus the ion density above the plate must also be larger than in the model. There is no mechanism for the ion velocity to be increased above the value determined from the potential drop. Using the measured current density in the sheath models results in a smaller calculated sheath thickness; however, the ion density is then inconsistent with the electron density at larger distances from the plate.

IV. SUMMARY AND CONCLUSION

The collisional sheath theory of Riemann has been combined with the charging theory for dust grains to provide a model for grain levitation in terms of the experimental parameters n_e, T_e, and Φ_p, for plasmas with an ion temperature much less than the electron temperature. Numerical solutions show that there are no stable equilibria closer to the plate than about five Debye lengths. There is a stable equilibrium point at a greater distance for grains that are sufficiently small. An expression is found for the largest diameter grain that can be levitated.

Experiments performed in a weakly collisional argon discharge plasma indicate that Riemann's collisional model of the sheath provides a close description of the sheath potential profile for the least negative bias at which grains would levitate, ≈ -30 V (Fig. 8). In this case, monodisperse dust grains levitate at the height predicted from the combined theories for the collisional sheath and for grain charging. The maximum grain size that will levitate is in approximate agreement with that predicted by model. However, both the measured sheath profiles and levitation heights deviate increasingly from the model as the plate bias voltage is made more negative. The model also does not predict the increasing ion current and hence underestimates the ion density in the sheath. The ion density being larger than predicted is consistent with the measured sheath thickness being smaller than predicted, thus resulting in a lower experimental dust levitation height.

The ion current collected at the walls must equal the rate of generation of ions within the plasma and an accurate sheath model must include source terms.[13–16] As the plate bias is made more negative, the sheath expands and a larger fraction of the ions is collected at the plate and a correspondingly smaller fraction of the ions collected at the walls of the vacuum chamber. An accurate model for the sheath above a biased surface and for the levitation of grains above this surface will thus require a model for the sheath in which the collected ion current is not a small perturbation to the particle balance.

ACKNOWLEDGMENTS

The authors thank Zoltan Sternovsky for assistance with Langmuir probe analysis. M.H., A.A.S.G., and S.R. are also with the Center for Integrated Plasma Studies.

This research was supported by the National Aeronautics and Space Administration (Microgravity) and by the Department of Energy (Fusion Energy Sciences).

[1] For recent reviews of dusty plasma physics, see P. K. Shukla, Phys. Plasmas **8**, 1791 (2001); D. A. Mendis and M. Rosenberg, Annu. Rev. Astron. Astrophys. **32**, 419 (1994).
[2] H. Thomas, G. E. Morfill, V. Demmel, and J. Goree, Phys. Rev. Lett. **73**, 652 (1994).
[3] A. Melzer, T. Trottenberg, and A. Piel, Phys. Lett. A **191**, 301 (1994).
[4] J. H. Chu and L. I, Phys. Rev. Lett. **72**, 4009 (1994).
[5] H. M. Thomas and G. E. Morfill, Nature (London) **379**, 806 (1996).
[6] V. Nosenko, J. Goree, and Z. W. Ma, Phys. Rev. Lett. **88**, 135001 (2002).
[7] J. B. Pieper and J. Goree, Phys. Rev. Lett. **77**, 3137 (1996).
[8] D. Bohm, in *The Characteristics of Electrical Discharges in Magnetic Fields*, edited by A. Guthrie and R. Wakerling (McGraw-Hill, New York, 1949), Chap. 3.
[9] M. A. Lieberman and A. J. Lichtenberg, *Principles of Plasma Discharges and Materials Processing* (Wiley, New York, 1994), Chap. 6.
[10] T. E. Sheridan and J. Goree, Phys. Fluids B **3**, 2796 (1991).
[11] K.-U. Riemann, J. Phys. D **24**, 493 (1991).
[12] K.-U. Riemann, Phys. Plasmas **4**, 4158 (1997).
[13] G. A. Emmert, R. M. Wieland, A. T. Mense, and J. N. Davidson, Phys. Fluids **23**, 803 (1980).
[14] V. Godyak and N. Sternberg, Phys. Plasmas **9**, 4427 (2002).
[15] R. J. Procassini, C. K. Birdsall, and E. C. Morse, Phys. Fluids B **2**, 3191 (1990).
[16] L. A. Schwager and C. K. Birdsall, Phys. Fluids B **2**, 1057 (1990).
[17] V. A. Godyak and N. Sternberg, IEEE Trans. Plasma Sci. **18**, 159 (1990).
[18] S. V. Vladimirov and N. F. Cramer, Phys. Rev. E **62**, 2754 (2000).
[19] R. Warren, Phys. Rev. **98**, 1658 (1955).
[20] H. Mott-Smith and I. Langmuir, Phys. Rev. **28**, 727 (1926).
[21] I. B. Bernstein and I. N. Rabinowitz, Phys. Fluids **2**, 112 (1959).
[22] T. Nitter, Plasma Sources Sci. Technol. **5**, 93 (1996).
[23] R. Hegerberg, M. T. Elford, and H. R. Skullerud, J. Phys. B **15**, 797 (1982).
[24] C. Arnas, M. Mikikian, and F. Doveil, Phys. Rev. E **60**, 7420 (1999).
[25] C. Arnas, M. Mikikian, G. Bachet, and F. Doveil, Phys. Plasmas **7**, 4418 (2000).
[26] D. Diebold, N. Hershkowitz, A. D. Bailey III, M. H. Cho, and T. Intrator, Rev. Sci. Instrum. **59**, 270 (1988).
[27] L. Oksuz and N. Hershkowitz, Phys. Rev. Lett. **89**, 145001 (2002).
[28] N. Hershkowitz, Bull. Am. Phys. Soc. **46**, 22 (2001).
[29] S. Meassick, M. H. Cho, and N. Hershkowitz, IEEE Trans. Plasma Sci. **PS-13**, 115 (1985).
[30] G. Bachet, L. Chérigier, and F. Doveil, Phys. Rev. Lett. **89**, 145001 (2002).
[31] J. A. Meyer, G.-H. Kim, M. J. Goeckner, and N. Hershkowitz, Plasma Sources Sci. Technol. **1**, 147 (1992).
[32] J. R. Smith, N. Hershkowitz, and P. Coakley, Rev. Sci. Instrum. **50**, 210 (1979).
[33] A. A. Sickafoose, J. E. Colwell, M. Horányi, and S. Robertson, J. Geophys. Res. **107** (A11), 1408, doi:10.1029/2002JA009347 (2002).